

Nanoporous characteristics of sol-gel-derived ZnO thin film

Anees A. Ansari^{1,†}, M. A. M. Khan¹, M. Alhoshan^{1,2}, S. A. Alrokayan¹, and M. S. Alsalhi¹

¹King Abdullah Institute for Nanotechnology, King Saud University, Riyadh-11451, P.O. Box-2454, Saudi Arabia

²Department of Chemical Engineering, King Saud University, P.O. Box 800, Riyadh 11421, Saudi Arabia

Abstract: Sol-gel-derived nanoporous ZnO film has been successfully deposited on glass substrate at 200 °C and subsequently annealed at different temperatures of 300, 400 and 600 °C. Atomic force micrographs demonstrated that the film was crack-free, and that granular nanoparticles were homogeneously distributed on the film surface. The average grain size of the nanoparticles and RMS roughness of the scanned surface area was 10 nm and 13.6 nm, respectively, which is due to the high porosity of the film. Photoluminescence (PL) spectra of the nanoporous ZnO film at room temperature show a diffused band, which might be due to an increased amount of oxygen vacancies on the lattice surface. The observed results of the nanoporous ZnO film indicates a promising application in the development of electrochemical biosensors due to the porosity of film enhancing the higher loading of biomacromolecules (enzyme and proteins).

Key words: nanoporous ZnO thin film; UV/visible absorption; photoluminescence

DOI: 10.1088/1674-4926/33/4/042002

EEACC: 2520

1. Introduction

Zinc oxide (ZnO) has received considerable attention because of its unique optical, electrical, mechanical, magnetic and piezoelectric properties. Nanostructured ZnO material exhibits interesting properties including, high catalytic efficiency and oxygen storage capability^[1–3]. Being a wide band gap (3.37 eV) semiconductor with large exciton binding energy (60 meV), ZnO has a lot of potential applications such as in field emission (FE) devices^[4], optoelectronics^[5], piezoelectric sensors^[6], biosensor devices^[7–9], transducers and resonators^[10]. Due to its high electro-catalytic activity, piezoelectricity and strong oxygen storage ability, ZnO has been considered as an attractive material for the fabrication of electrochemical devices. The electro-catalytic behavior of nanostructured ZnO can be tuned by surface modification. Moreover, controlling/tailoring the surface morphology or grain size is an important characteristic of ZnO films for their effective applications in particular technology development. Therefore, the ability to build oriented assemblies of 1-D nanostructure ZnO is also especially attractive for the fabrication of future electrochemical nano-devices. In this regard, a number of attempts have been made to fabricate one-dimensional ZnO nanostructures including thermal evaporation^[10], vapor-phase transport^[12], laser ablation^[13], metal-organic chemical vapor deposition^[14] and the sol-gel chemical process^[15]. Several reports have been published in the literature on fabrication, optical and structural characterization of nanostructured ZnO thin films by using the sol-gel method^[16–19]. Li and Gao^[20] reported ZnO nanocomposite films deposited onto glass substrates by magnetron sputtering in different atmospheres. Kale and Lu^[21] reported ZnO microrods deposited by hydrothermal method and they studied the structural, optical and morphological properties. Wu and Pan^[22] reported ZnO nanofibers prepared by the electrospinning technique. Among these methods, the sol-gel dip-

coating method has distinct advantages due to its cost effectiveness, simplicity, excellent compositional control, homogeneity and low temperature processing. Sol-gel-derived films exhibit high porosity, large surface energy and biocompatibility that is applicable in biosensor applications for higher loading of enzymes on the electrode surface. The high porosity of the films is due to an increased surface roughness, which improves after biomacromolecule immobilization.

In the present paper, we report a very facile and effective method for developing nanoporous ZnO film by using a sol-gel process via the dip-coating technique, study their optical, structural properties and further investigate the effect of annealing on the optical properties of nanoporous ZnO thin film. The fabrication of sol-gel-derived nanoporous thin films are highly applicable in the development of electrochemical biosensing devices.

2. Experimental details

2.1. Preparation

Firstly, 2 g zinc acetate dihydrate [$\text{Zn}(\text{CH}_3\text{COO})_2 \cdot 2\text{H}_2\text{O}$, Merck, Germany] was dissolved in 10 mL distilled de-ionized water. To achieve a uniform coating on the glass, substrate ethylene glycol [Merck, Germany] was added into the resulting solution for transparent gelation formation. A glass substrate was used for film fabrication, which was carefully pre-cleaned with chromic acid, liquid laboratory detergent and water. The substrate (glass) was further cleaned with de-ionized water, washed with acetone and dried. The film was deposited onto the glass substrate using a dip-coating process with a selected pulling speed of 10 cm/min. The prepared film was dried at 200 °C and afterward heated at 300, 400 and 600 °C for 1 h^[1, 2, 23].

† Corresponding author. Email: aneesaansari@gmail.com

Received 11 September 2011, revised manuscript received 25 October 2011

© 2012 Chinese Institute of Electronics

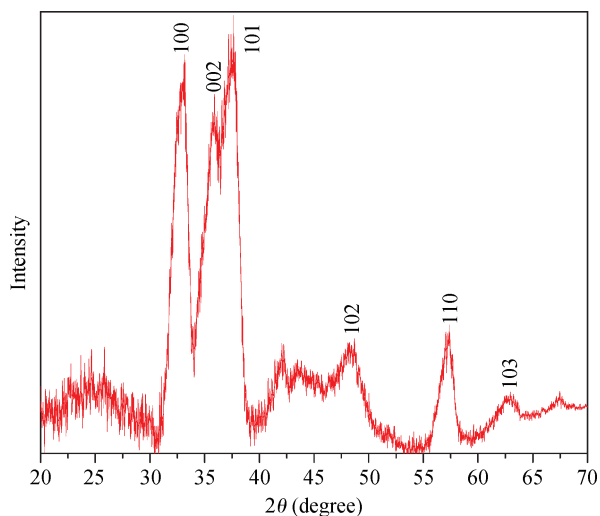
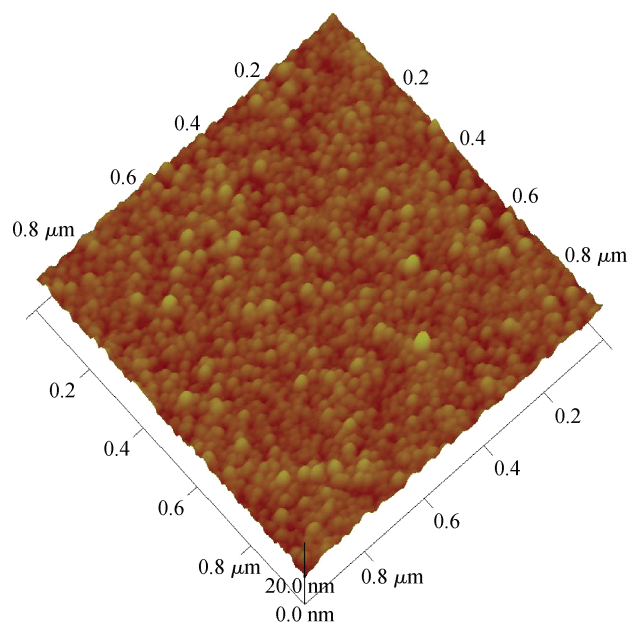


Fig. 1. X-ray diffraction pattern of sol-gel-derived nanoporous ZnO thin film.



2.2. Characterization of the prepared nanoporous film

Atomic force micrograph (AFM) Veeco DICP2 studies were conducted to examine the surface topography of the film. Absorption spectra of ZnO film were recorded in the 200–600 nm range using a Perkin-Elmer UV-visible spectrophotometer. The prepared film was further characterized by using a photoluminescence spectrophotometer. Photoluminescence measurements were done at room temperature in the 300–800 nm range using a Perkin Elmer LS055 spectrometer using an excitation wavelength of 250 nm.

3. Results and discussion

The XRD diffraction pattern (Fig. 1) shows the crystallographic phase present in the sol-gel-derived ZnO film deposited on glass substrate. The deposited film shows all diffraction planes such as (100), (002), (101), (102), (110), (103) and (112), which correspond to a hexagonal wurtzite ZnO structure and well-matches the standard (JCPDS #751526) data^[23]. The ZnO film coated onto glass substrate shows three strong diffraction peaks at (100), (002) and (101), indicating the distribution of ZnO grains in the film along different directions. This may be attributed to optimized deposition and annealing of the ZnO film. The diffraction peaks of ZnO are broad, suggesting a smaller crystalline size of ZnO. The average crystallite size of the ZnO film calculated by Scherrer's equation is 8–10 nm.

The surface topography of the sol-gel-derived ZnO thin film was examined by AFM micrographs, as shown in Fig. 2. The AFM image shows that the film is crack-free and spherical nanoparticles are uniformly distributed. Grains are tightly packed and the average crystalline size varies from 10 nm. The average surface roughness root mean square (RMS) of the sol-gel ZnO film is determined to be 13.8 nm, indicating high porosity. The high surface roughness of the film might originate from the decrease in the grain size due to annealing effect that increases the photo-catalytic activity of the film. Similar observations have made by Yang *et al.*^[24]. The granular struc-

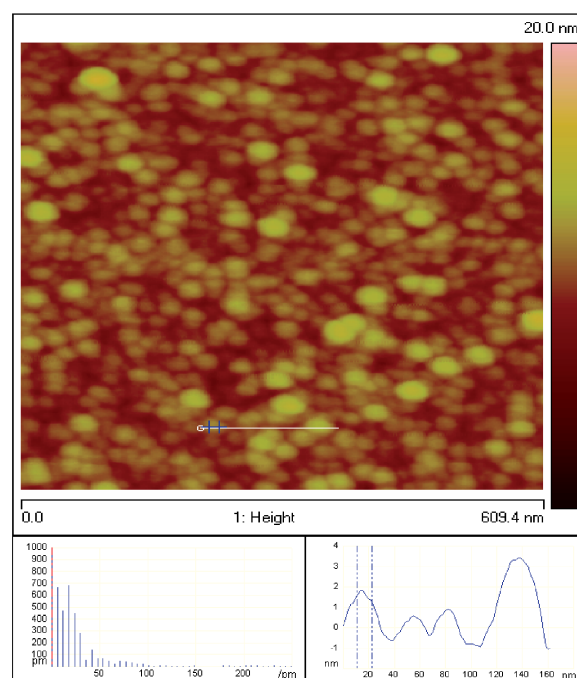


Fig. 2. AFM images of sol-gel-derived nanoporous ZnO thin film.

ture existing in the film may be due to thinner film. The thickness of the nanoporous ZnO film is 50 nm.

UV-visible absorption spectra were employed for characterization of the sol-gel-derived nanoporous ZnO film. The fabricated film was annealed at different temperatures for measurement of the annealing effect on optical properties. The absorption spectra of the sol-gel-derived nanoporous ZnO film show a diffused direct band in the UV region (200–400 nm). The absorption edges of the nanoporous ZnO films spectra are red shifted as the annealing temperature is increased regularly from 200 to 400 °C. Whereas, the sample 4 annealed film at 600 °C shows a blue shift, which might be due to the quantum size effect caused by decreasing the crystal size (Fig. 3)^[23–26].

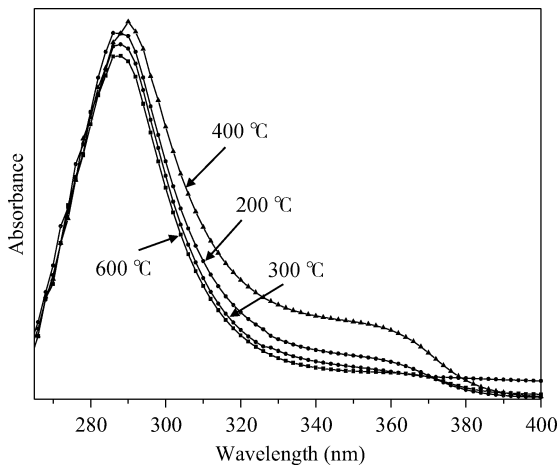


Fig. 3. UV/visible spectra of sol-gel-derived nanoporous ZnO thin film.

3.1. Optical properties

The effect of annealing temperature (200, 300, 400 and 600 °C) on the optical properties of sol-gel-derived nanoporous ZnO thin film was observed as shown in Figs. 4–7. A significant difference is observed in the optical spectra of the ZnO film at different annealing temperatures. The observed absorption spectral results show that the films are transparent in the visible region. The absorbance edge of the spectrum (absorption or transmittance) being shifted after heat treatment might be due to the size confinement effect on the optical behavior of nanoporous ZnO thin film. The energy band-gap, transmittance, reflectance and refractive index are changed after heat treatment at different temperatures because of the semiconducting behavior of the material, which are the fundamental parameters of the materials. The optical transmittance spectra of ZnO thin films are shown in Fig. 4. The optical transmittance of the films increases with increases in annealing temperature. The absorption coefficient (α) can be calculated using the equation^[26–28]:

$$\alpha = \ln(1/T)/d, \tag{1}$$

where T is the transmittance and d is the film thickness.

The theory of optical absorption gives the relationship between the absorption coefficient (α) and the photon energy ($h\nu$) for direct allowed transition as^[29]

$$\alpha h\nu = A(h\nu - E_g)^m, \tag{2}$$

where $h\nu$ is the photon energy, E_g is the band gap and A is a constant having separate values for different transitions. In the above equation $m = 1/2$ for a direct allowed transition, $m = 3/2$ for a direct forbidden transition, $m = 2$ for an indirect allowed transition and $m = 3$ for an indirect forbidden transition. After fitting all the values of m in the above relation, the value equal to $1/2$ is found to hold well, leading to direct transitions. Figure 5 shows the plots of $(\alpha h\nu)^2$ versus $h\nu$ for the thin films deposited on glass substrate. The values of E_g^{opt} have been estimated by taking the intercept of the extrapolations to zero absorption with the photon energy axis i.e. $(\alpha h\nu)^2 \rightarrow 0$. The values of E_g^{opt} for various films at different annealing temperatures

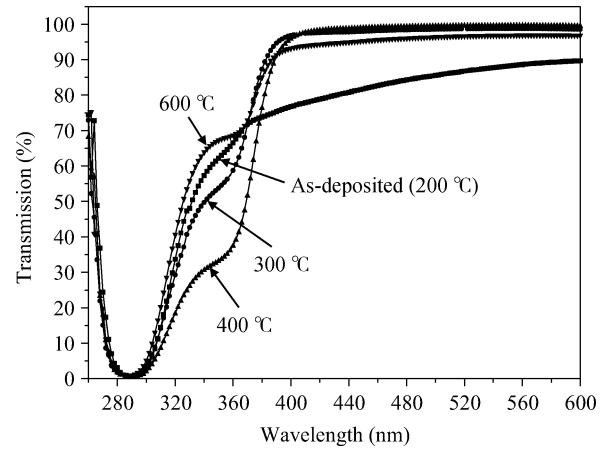


Fig. 4. Transmittance (T) with wavelength at different temperatures of nanoporous ZnO thin film.

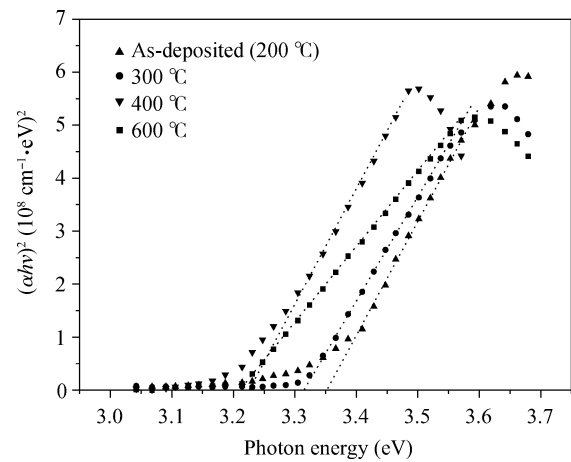


Fig. 5. $(\alpha h\nu)^2$ versus $h\nu$ at different temperatures of nanoporous ZnO thin film.

are shown in Table 1. It is clear from the table that the energy band gap decreases from 3.35 to 3.21 eV with increasing the annealing temperature from 200 to 600 °C, respectively. This suggests that the absorption edge shifts to the lower energy as a consequence of the thermal annealing on film and the fundamental absorption edge corresponds to a direct energy gap. The decreases in optical band gap means that the temperature affects the optical band gap by changing atomic distances. The change in the optical band gap may be attributed to a decrease of the optical band gap due to interatomic distances with increasing changes. The decrease in optical band gap increases the width of the energy bands and that is why the optical band gap decreases. Annealed films exhibit strong red shift in their optical spectra due to the localization of charge carriers in individual nanocrystals^[10, 17–19]. This is attributed to the grain size-dependent properties of the energy band gap. Similar red shift in energy band gap E_g values for the films with smaller thickness and/or grain sizes have been reported for chemically deposited thin films^[30, 31].

Figures 6 and 7 show the refractive index, n and the extinction coefficient k as functions of wavelength and annealing temperature. After annealing the film, k decreased at wavelengths below the band gap with annealing temperature. Such

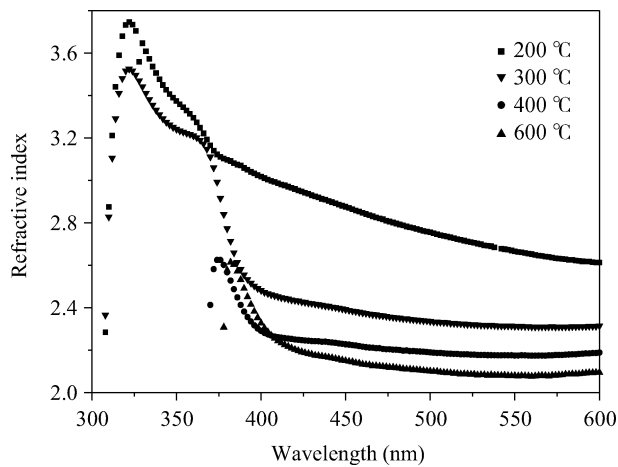


Fig. 6. Refractive index (n) versus wavelength at different temperatures of nanoporous ZnO thin film.

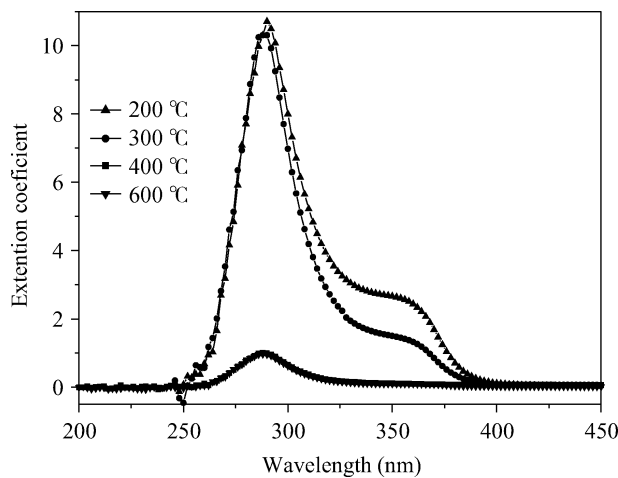


Fig. 7. Extinction coefficient (k) versus wavelength at different temperatures of nanoporous ZnO thin film.

decrease indicates weaker photon absorption by electrons transitions across the band gap, where less intermediate defect levels could be present after annealing. Liu *et al.*^[32] studied the influence of annealing on the optical properties of FVAD ZnO films as a function of annealing time. In their case, n decreased significantly with annealing temperature. The refractive indices and extinction coefficient of as-deposited (200 °C), 300, 400 and 600 °C annealed films are given in Table 1. Similar results have been observed in other reports^[33, 34].

The refractive index of the film was calculated by the following relation:

$$R = (n + 1)^2 + K^2 / (n + 1)^2 + K^2, \quad (3)$$

where k ($k = \alpha \lambda / 4\pi$) is the extinction coefficient.

The fundamental electron excitation spectrum of the nanoporous ZnO film is examined by means of a frequency dependence of the complex electronic dielectric constant. The dielectric constant is defined as, $\epsilon(\omega) = \epsilon_1(\omega) + i\epsilon_2(\omega)$ and the real and the imaginary parts of the dielectric constant are related to the n and k values. The relationships between the two pairs of quantities ($n, k, \epsilon_1, \epsilon_2$) are given by the following

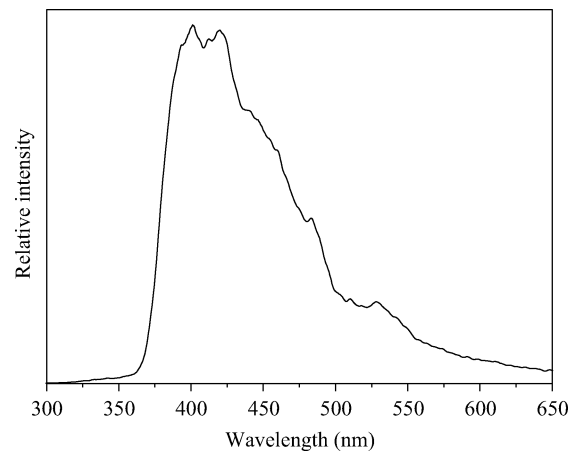


Fig. 8. Photoluminescence spectrum of sol-gel-derived nanoporous ZnO thin film.

Table 1. Optical parameters for as-deposited and annealed ZnO thin film.

ZnO	n	k	ϵ_1	ϵ_2	E_g (eV)
As-deposited (200 °C)	2.72	0.051	7.37	0.275	3.35
300 °C	2.18	0.047	4.75	0.205	3.32
400 °C	2.09	0.013	4.37	0.054	3.23
600 °C	2.32	0.012	5.39	0.059	3.21

formulas:

$$\begin{aligned} \epsilon_1 &= n^2 - k^2, \\ \epsilon_2 &= 2nk. \end{aligned} \quad (4)$$

The values of these two parameters with fixed photon energy and different temperatures are given in Table 1. It can be seen that both the real ϵ_1 and the imaginary part ϵ_2 of the dielectric constant decreases with increasing the annealing temperature.

3.2. Photoluminescence spectra

Figure 8 shows the results of the photoluminescence (PL) spectra of sol-gel-derived nanoporous ZnO film deposited on glass substrate carried out at room temperature. The PL emission spectrum was obtained under ultraviolet excitation at 255 nm. The PL spectrum reveals significant information about the lattice defect and illustrates potential applications in optoelectronic devices. Two diffused PL emission bands are measured, one is between 300–550 nm with two splitting peaks and another one maxima at 678 nm. The UV emissions at 366, 400 and 415 nm correspond to the recombination of free excitons between the conductive band and the valence band of ZnO, and is called near-band-edge emission, is well known that visible luminescence mainly originates from defect states such as Zn interstitials and oxygen vacancies, etc^[35–37]. It is generally true that annealing in vacuum causes the film to lose oxygen and helps create oxygen deficient type defects, as partially confirmed by our UV/visible spectra and AFM analysis. A red emission band at 678 nm (eV) is attributed to the transition between the vacancy of oxygen and interstitial oxygen, and these

defects should be more likely to be limited to surfaces and interfaces. The appearance of a dominant UV emission band indicates the crystal quality of the deposited nanoporous ZnO thin film^[37, 38].

4. Conclusion

Sol-gel-derived nanoporous ZnO films were deposited on glass substrate by using a dip-coating process. AFM images exhibited that the ZnO film was crack-free, porous in nature and the surface roughness (RMS) was determined to be 13.6 nm, indicating high porosity. It was found from the UV/visible spectra that the energy band gap increases as the annealing temperature increases, and this might be due to the size effect. Optical band gap and optical constants (refractive index, extinction coefficient, real and imaginary parts of the dielectric constant) of nanoporous ZnO film were also determined. These observed results signify that the high porosity of sol-gel-derived nanoporous ZnO thin film is appropriate for loading high enzyme quantities to fabricate sensitive electrochemical biosensor devices. The high porosity of the films is likely to embed a large concentration of oxygen at the grain boundaries or interstitial sites, thereby changing the microstructure of the deposited film. These features play a vital role in the fabrication of electrochemical biosensor applications.

References

- [1] Pan Z W, Dai Z R, Wang Z L. Nanobelts of semiconducting oxides. *Science*, 2001, 291(5510): 1947
- [2] Park J Y, Song D E, Kim S S. An approach to fabricating chemical sensors based on ZnO nanorod arrays. *Nanotechnology*, 2008, 19(10): 105503
- [3] Goldberger J, Sirbuly D J, Law M, et al. ZnO nanowire transistors. *J Phys Chem B*, 2005, 109(1): 9
- [4] Lee C J, Lee T J, Lyu S C, et al. Field emission from well-aligned zinc oxide nanowires grown at low temperature. *Appl Phys Lett*, 2002, 81(19): 3648
- [5] Sun H, Zhang Q F, Wu J L. Electroluminescence from ZnO nanorods with an n-ZnO/p-Si heterojunction structure. *Nanotechnology*, 2006, 17(9): 2271
- [6] Arnold M S, Avouris P, Pan Z W, et al. Field-effect transistors based on single semiconducting oxide nanobelts. *J Phys Chem B*, 2003, 107(3): 659
- [7] Ansari A A, Kaushik A, Solanki P R, et al. Sol-gel derived nanoporous cerium oxide film for application to cholesterol biosensor. *Electrochem Commun*, 2008, 10(9): 1246
- [8] Ansari A A, Kaushik A, Solanki P R, et al. Electrochemical cholesterol sensor based on tin oxide-chitosan nanobiocomposite film. *Electroanalysis*, 2009, 21(8): 965
- [9] Ansari A A, Solanki P R, Malhotra B D. Sol-gel derived nanostructured cerium oxide film for glucose sensor. *Appl Phys Lett*, 2008, 92(26): 263901
- [10] Klingshirm C. ZnO: material, physics and applications. *Chem Phys Chem*, 2007, 8(6): 782
- [11] Shen G Z, Bando Y, Liu B D, et al. Characterization and field-emission properties of vertically aligned ZnO nanonails and nanopencils fabricated by a modified thermal-evaporation process. *Adv Funct Mater*, 2006, 16(3): 410
- [12] Wang R C, Liu C P, Huang J L, et al. ZnO nanopencils: efficient field emitters. *Appl Phys Lett*, 2005, 87(1): 013110
- [13] Okada T, Kawashima K, Nakata Y. Nano-wire pig-tailed ZnO nano-rods synthesized by laser ablation. *Thin Solid Films*, 2006, 506: 274
- [14] Zhong J, Chen H, Saraf G, et al. Integrated ZnO nanotips on GaN light emitting diodes for enhanced emission efficiency. *Appl Phys Lett*, 2007, 90(20): 203515
- [15] Yu L G, Zhang G M, Li S Q, et al. Fabrication of arrays of zinc oxide nanorods and nanotubes in aqueous solution under an external voltage. *J Cryst Growth*, 2007, 299(1): 184
- [16] Srinivasan G, Kumar J. Optical and structural characterisation of zinc oxide thin films prepared by sol-gel process. *Cryst Res Technol*, 2006, 41: 893
- [17] Zhang Y, Lin B, Sun X, et al. Temperature-dependent photoluminescence of nanocrystalline ZnO thin films grown on Si (100) substrates by the sol-gel process. *Appl Phys Lett*, 2005, 86(13): 131910
- [18] Caglar M, Ilican S, Caglar Y, et al. Electrical conductivity and optical properties of ZnO nanostructured thin film. *Appl Surf Sci*, 2009, 255(8): 4491
- [19] Dev A, Panda S K, Kar S, et al. Surfactant-assisted route to synthesize well-aligned ZnO nanorod arrays on sol-gel-derived ZnO thin films. *J Phys Chem B*, 2006, 110(29): 14266
- [20] Li Z W, Gao W. Growth of zinc oxide thin films and nanostructures by wet oxidation. *Thin Solid Films*, 2007, 515(7/8): 3323
- [21] Kale R B, Lu S Y. Structural, morphological, and optical properties of double-ended needle-like ultra-long ZnO micro/nanorods. *J Phys Condens Mater*, 2007, 19(9): 096209
- [22] Wu H, Pan W. Preparation of zinc oxide nanofibers by electrospinning. *J Am Ceram Soc*, 2006, 89(2): 699
- [23] Ansari A A. Optical and structural properties of sol-gel derived nanostructured CeO₂ film. *Journal of Semiconductors*, 2010, 31(5): 053001
- [24] Yang J L, An S J, Park W I, et al. Photocatalysis using ZnO thin films and nanoneedles grown by metal-organic chemical vapor deposition. *Adv Mater*, 2004, 16 (18): 1661
- [25] Irimpan L, Nampoori V P N, Radhakrishnan P, et al. Size dependent fluorescence spectroscopy of nanocolloids of ZnO. *J Appl Phys*, 2007, 102(6): 063524
- [26] Ansari A A, Singh S P, Malhotra B D. Optical and structural properties of nano-structured CeO₂:Tb³⁺ film. *J Alloys and Compounds*, 2011, 509(2): 262
- [27] Rubin K A, Chen M. Progress and issues of phase-change erasable optical recording media. *Thin Solid Films*, 1989, 181(1/2): 129
- [28] Gosain D P, Shimizu T, Ohmura M, et al. Some properties of Sb₂Te_{3-x}Se_x for nonvolatile memory based on phase transition. *J Mater Sci*, 1991, 26(12): 3271
- [29] Khan M A M, Zulfequar M, Hussain M. Optical investigation of a-Se_{100-x}Bi_x alloys. *Opt Mater*, 2003, 22(1): 21
- [30] Tauc J, Grigorovici R, Vancu A. Optical properties and electronic structure of amorphous germanium. *Phys Status Solidi*, 1966, 15(2): 627
- [31] Shinde V R, Lokhande C D, Mane R S, et al. Hydrophobic and textured ZnO films deposited by chemical bath deposition: annealing effect. *Appl Surf Sci*, 2005, 245(1-4): 407
- [32] Kale R B, Lokhande C D. Influence of air annealing on the structural, optical and electrical properties of chemically deposited CdSe nano-crystallites. *Appl Surf Sci*, 2004, 223(4): 343
- [33] Liu Y C, Tung S K, Hsieh J H. Influence of annealing on optical properties and surface structure of ZnO thin films. *J Cryst Growth*, 2006, 287(1): 105
- [34] David T, Goldsmith S, Boxman R L. Electro-optical and structural properties of thin ZnO films, prepared by filtered vacuum

- arc deposition. *Thin Solid Films*, 2004, 447(1): 61
- [35] Mastro M A, Freitas J A Jr, Eddy C R Jr, et al. Luminescence characteristics of zinc oxide nanocrystals deposited on glass via a solution method. *Physica E*, 2009, 41(3): 487
- [36] Greene L, Law M, Goldberger J, et al. Low-temperature wafer-scale production of ZnO nanowire arrays. *Angew Chem Int Ed*, 2003, 42(26): 3031
- [37] Umar A, Karunakaran B, Suh E K, et al. Structural and optical properties of single-crystalline ZnO nanorods grown on silicon by thermal evaporation. *Nanotechnology*, 2006, 17(16): 4072